A Notch Filter for Magnetically Suspended Rotors Based on Rotating Coordinate Transformation

Shiqiang Zheng[a], Rui Feng [b]

[a] School of Instrumentation Science & Opto–electronics Engineering, Beijing University of Aeronautics and Astronautics, No.37 Xueyuan Road, Beijing 100191, China, zhengshiqiang@buaa.edu.cn
[b] Huawei Technologies Co. Ltd, No.156, Beiqing Road, Beijing 100095, China

***Abstract*—Synchronous vibration are obstacles to the performance improvement of a rotating shaft supported by active magnetic bearings (AMBs). Based on the synchronous rotating coordinate transformation, this paper proposed a novel notch filter for the autobalancing of magnetically suspended rotors. After the analysis of the frequency characteristics of the novel notch filters, the calculating method of the convergence rate and comparison with the traditional notch filter are further investigated. Finally, the corresponding simulations and experiments are conducted. The results demonstrate that the novel notch filter has a good significant effect on the synchronous vibration of weakly gyroscopic rotors.**

I. INTRODCUTION

The basic idea of autobalancing control is introduced by Burrows et al, and a great number of the different techniques have been proposed to achieve this task, which can be divided into two categories. One approach is to estimate position of the rotor's principal axis of inertia and force the magnetically suspended rotor to rotate about the principal axis of inertia, named zero displacement. However, this approach depends on the accuracy of identification results of the system model, and will result in the housing vibrations. The other one, called zero magnetic force, is to eliminate synchronous force generated by magnetic bearings, which is based on the self-alignment theory. Different approaches, such the notch filter (Hui et al., 2010), adaptive feedforward (Knospe et al., 1996), and robust control (Kuseyri, 2012), have been proposed to eliminate the synchronous components in the currents of magnetic bearings. The two-modulation-step implementation of the generalized notch filters was introduced by Raoul Herzog (1996) and sensitivity function was used to analyze the stability of the closed-loop system with notch filters (Raoul Herzog et al., 1996), which is wildly considered as an effective approach.

Based on the relationships between two synchronous sinusoidal vibration forces and signals along the radial axes, which are caused by residue mass unbalance, this paper proposes a novel kind of notch filter using synchronous rotating coordinator transform. The main idea of this paper is that: (1) After being transformed by the synchronous rotating coordinator, the phases of synchronous spatial vectors (force, displacement, etc) become static, that is, the synchronous vectors become zero-frequency vectors; (2) The zero-frequency vectors can be extracted by passing through the low-pass filters; (3) The synchronous vectors can be retrieved by the extracted zero-frequency vectors and inverse synchronous rotating coordinator transform.

II. NOVEL NOTCH FILTER BASED ON SYNCHRONOUS ROTATING COORDINATE TRANSFORM

A. Principle

Assuming that the cross section of the rotor shaft is an ideal round and the generalized controlled channels adopted in the four degree of radial magnetic bearings are identical, the vibration signals of X-channel and Y-channel have the same amplitude and frequency, but with a phase difference of 90 degrees.

As shown in Figure 1, Let M and C denote the geometric centre and mass centre of the rotor, respectively. The fixed coordinate system CX_sY_s denotes the position sensor frame. CX_rY_r denotes the rotating coordinate system with a spin rate of Ω. When the rotor rotates stably around its inertial axis of the rotor, the trajectory of the geometric center is a circle with the center C and the eccentricity ε. Let $(x_s, y_s)^{\mathrm{T}}$ and $(x_r, y_r)^{\mathrm{T}}$ denote the motion of M in the fixed coordinate system and rotating coordinate system, respectively, we can get

$$\begin{pmatrix} x_r \\ y_r \end{pmatrix} = \boldsymbol{T}(\Omega t)\begin{pmatrix} x_s \\ y_s \end{pmatrix} = \begin{pmatrix} \cos(\Omega t+\theta) & \sin(\Omega t+\theta) \\ -\sin(\Omega t+\theta) & \cos(\Omega t+\theta) \end{pmatrix}\begin{pmatrix} x_s \\ y_s \end{pmatrix} \quad (1)$$

where $\boldsymbol{T}(\Omega t)$ is the the synchronous rotating coordinate transformation matrix; θ is the phase compensation angle. In fact, M is the constant vector in the rotating coordinate system. So $(x_r, y_r)^{\mathrm{T}}$ is frequency zero (DC) displacement vector, and can be filtered out by a low-pass filter. Through a multiplication by the inverse synchronous rotating coordinate transformation matrix $\hat{\boldsymbol{T}}(\Omega t)$, namely,

$$\begin{bmatrix} x_c \\ y_c \end{bmatrix} = \hat{\boldsymbol{T}}(\Omega t)\begin{bmatrix} x_r \\ y_r \end{bmatrix} = \begin{bmatrix} \cos(\Omega t) & -\sin(\Omega t) \\ \sin(\Omega t) & \cos(\Omega t) \end{bmatrix}\begin{bmatrix} x_r \\ y_r \end{bmatrix} \quad (2)$$

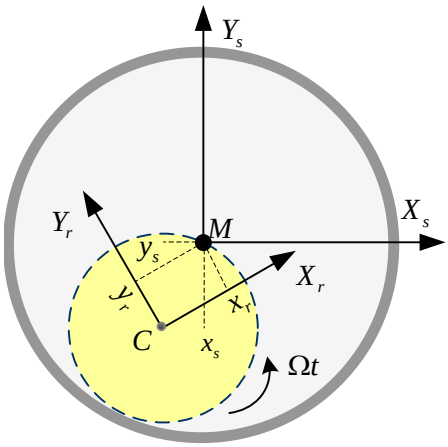

Figure 1. Schematic diagram of coordinate transformation

The DC displacement vector is shifted back to synchronous vibration signals, which need to be identified. This two-modulation procedure is shown in Figure 2.

Here we use the complex coefficient method to represent the displacement vector $(x, y)^{\mathrm{T}}$, transformation matrix $\boldsymbol{T}(\Omega t)$ and $\hat{\boldsymbol{T}}(\Omega t)$ by

$$\begin{aligned} d &= x + jy \\ \boldsymbol{T}(\Omega t) &= e^{-j(\Omega t+\theta)} \\ \hat{\boldsymbol{T}}(\Omega t) &= e^{j\Omega t} \end{aligned} \tag{3}$$

Set $\tilde{d}(j\omega)$, $\tilde{\boldsymbol{T}}(j\omega,\Omega)$ and $\tilde{\boldsymbol{T}}_{inv}(j\omega,\Omega)$ as the Fourier transformations of $d(t)$, $\boldsymbol{T}(\Omega t)$, $\boldsymbol{T}_{inv}(\Omega t)$, respectively. It can be derived that

$$\begin{cases} \tilde{\boldsymbol{T}}(j\omega,\Omega) = \delta(j\omega + j\Omega)e^{-j\theta} \\ \tilde{\boldsymbol{T}}_{inv}(j\omega,\Omega) = \delta(j\omega - j\Omega) \end{cases} \tag{4}$$

Meanwhile, it can also be achieved that

$$\begin{cases} F(d(t)*\boldsymbol{T}(\Omega t)) = \tilde{\boldsymbol{T}}(j\omega,\Omega)\otimes\tilde{d}(j\omega) = \tilde{d}(j\omega + j\Omega)e^{-j\theta} \\ F(d(t)*\boldsymbol{T}_{inv}(\Omega t)) = \tilde{\boldsymbol{T}}_{inv}(j\omega,\Omega)\otimes\tilde{d}(j\omega) = \tilde{d}(j\omega - j\Omega) \end{cases} \tag{5}$$

where $F(\cdot)$ and $\otimes$ denote the Fourier transformation and revolution operator, respectively. Assume the transfer function of the low-pass filter as $g_f(s)$, and combining with (1), (2) and (5), the transfer function of the band-pass filter shown in Figure 2 is given by

$$\begin{aligned} \hat{g}_n(s) &= \frac{\tilde{d}_{out}(s)}{\tilde{d}_{in}(s)} = \frac{\tilde{x}_{out}(s) + j\tilde{y}_{out}(s)}{\tilde{x}_{in}(s) + j\tilde{y}_{in}(s)} \\ &= \frac{\tilde{\boldsymbol{T}}_{inv}(j\omega,\Omega)\otimes(g_f(s)*\tilde{\boldsymbol{T}}(j\omega,\Omega)\otimes\tilde{d}_{in}(s))}{d_{in}(s)} \\ &= g_f(s - j\Omega)e^{-j\theta} \end{aligned} \tag{6}$$

Therefore, the transfer function of this novel notch filter can be achieved as

$$g_n(s) = \frac{1}{1+\hat{g}_n(s)} = \frac{1}{1+g_f(s-j\Omega)e^{-j\theta}} \tag{7}$$

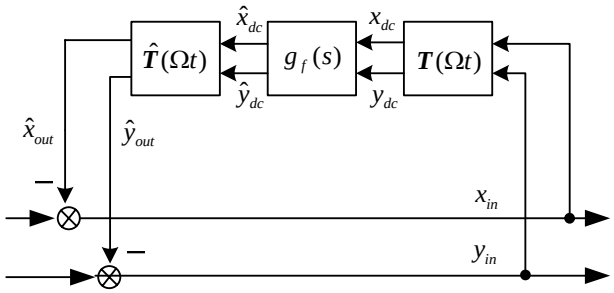

Figure 2. The implemetation principle of novel notch filter

B. *Performance Comparisons*

Usually, the classic notch filter has the following form

$$g_r(s) = \frac{s^2 + \varepsilon_1 s + \Omega^2}{s^2 + \varepsilon_2 s + \Omega^2} \tag{8}$$

When the first order low-pass filter is adopted, the novel notch filter is given as Eq. (8). The frequency response at the center frequency $j\Omega$ is $g_n(j\Omega) = \varepsilon/(\varepsilon + \kappa e^{-j\theta})$, and as for $j\omega = j(\sigma + \Omega)$ where $\sigma << \Omega$, it can resolved that

$$g_n(j(\Omega+\sigma)) = \frac{j(\Omega+\sigma) + \varepsilon - j\Omega}{j(\Omega+\sigma) + \varepsilon + \kappa e^{-j\theta} - j\Omega} = \frac{j\sigma + \varepsilon}{j\sigma + \varepsilon + \kappa e^{-j\theta}} \tag{9}$$

Thereby, it can be concluded that bandwidth and depth of the notch filters are decided by ε and κ, the influence of which are similar to the ε_1 and ε_2 in Eq. (8), respectively (as shown in Figure 3). While compared with the classic notch filter, $e^{-j\theta}$ in Eq. (8) not only leads to the free pole assignment of $g_n(s)$, but also affects the phase-frequency response in the frequencies adjacent to the center frequency Ω, which is essential to the system stability. The proposed notch filter has the same advantage as the two-modulation-step notch filter proposed by Herzog (1996), which can output the steady unbalance state in rotating coordinate without additional computation.

As for the signals $x = \gamma_1 \sin(\Omega t + \varphi_1)$ and $y = \gamma_2 \sin(\Omega t + \varphi_2)$, where $\gamma_1 \neq \gamma_1$ and $\varphi_1 - \varphi_1 \neq \pi/2$, we have that

$$\begin{aligned} x + jy &= \gamma_1 \frac{e^{j(\Omega t+\varphi_1)} - e^{-j(\Omega t+\varphi_1)}}{2j} + \gamma_2 \frac{e^{j(\Omega t+\varphi_2)} - e^{-j(\Omega t+\varphi_2)}}{2j} \\ &= \hat{\gamma}_1 e^{j\Omega t} + \hat{\gamma}_2 e^{-j\Omega t} \end{aligned} \tag{10}$$

where $\hat{\gamma}_1 = -j(\gamma_1 e^{j\varphi_1} + \gamma_2 e^{j\varphi_2})/2$ and $\hat{\gamma}_2 = -j(\gamma_1 e^{-j\varphi_1} + \gamma_2 e^{-j\varphi_2})/2$.

Based on the frequency characteristics of $g_n(s)$, the power of $\hat{\gamma}_1 e^{j\Omega t}$ will be greatly attenuated and that of $\hat{\gamma}_2 e^{-j\Omega t}$ will remain invariant when $x + jy$ passes though $g_n(s)$, while both of $\hat{\gamma}_1 e^{j\Omega t}$ and $\hat{\gamma}_2 e^{-j\Omega t}$ will be attenuated by passing through $g_r(s)$.

TABLE I. THE SIMULATION PAREMETER OF NOTCH FILTER

Parameters	Values
ε	8π
κ	36π
θ	0
ε_1	42
ε_2	210
Ω	500Hz

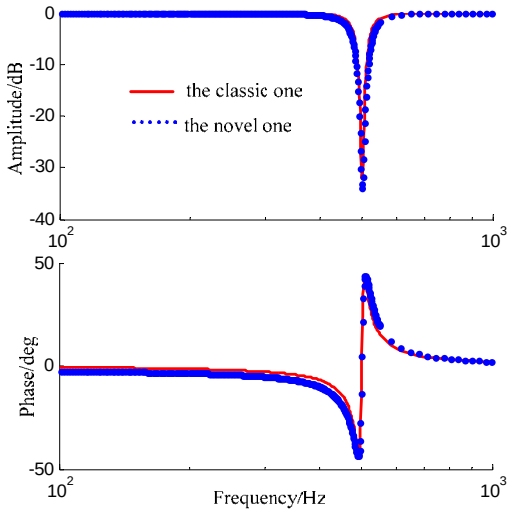

Figure 3. The Bode diagram of notch filter

III. IMPLEMENTATION

A. Control Scheme

To evaluate the effectiveness of the proposed method, experiments were carried out on an AMB based compressor test rig, which is fixed vertically on a metal base (as shown in Figure 4). The design parameters of this test rig are listed in Table 1.

Figure 4. AMB test rig

TABLE II. DESIGN PARAMETERS OF AMB TEST RIG

Name	Value	Unit
Length of the rotor	554	mm
Mass of the rotor	6.85	kg
Power	4	kW
The first bending frequency	650	Hz
The transverse moment of inertia	0.1147	kg m^2
The polar moment of inertia	0.002529	kg m^2
Bias current	1.2	A
Current stiffness	43	N A^{-1}
Negative position stiffness	-0.21×10^6	N m^{-1}
Radial protective clearance	0.2	mm

In this paper, the inverse power amplifier model in feedforward channel is also introduced to compensate the displacement stiffness force to improve the accuracy of the synchronous displacement stiffness force compensation. The schematic diagram of the AMB control system combined with the novel notch filter is shown in Figure 5.

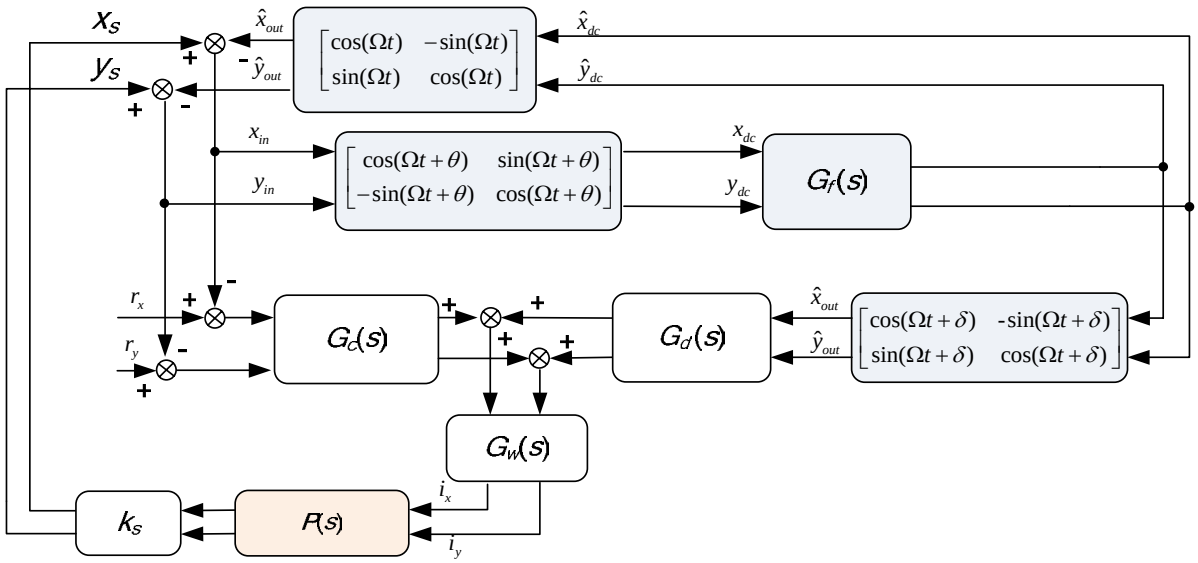

Figure 5. Vibration control scheme used for this paper

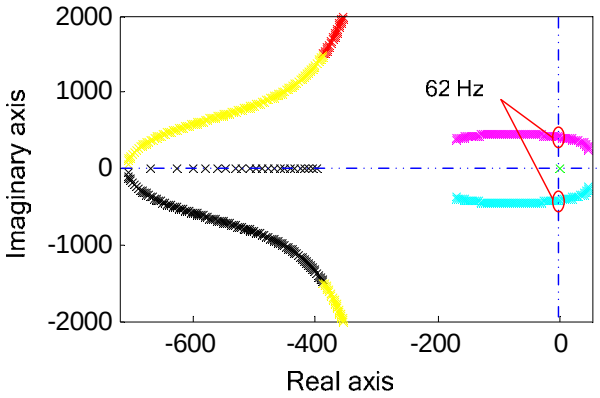

Figure 6. Stability analysis: dominant root locus

Stability is the primary concern, among the other specifications due to the energy and speed of the high-speed rotating machinery. For the linearized high-speed AMB-rotor system, the closed-loop root locus is widely employed in the controller design for its simplicity. Figure 6 reveals the dominant root locus when Ω varies from 20Hz to 800Hz with the control scheme shown in Figure 5. It can be seen that the system is stable if Ω >62Hz. Since the AMB rotor system runs at a speed of 30000r/min in this paper, stability of the system can meet the operation requirements.

B. Experiments

In order to evaluate the proposed compensation scheme, an AMB test rig as shown in Figure 4 is used to test compensation scheme performance on the synchronous vibration reduction. Vibration signals are obtained by an acceleration sensor mounted on the motor base.

Vibration acceleration signal spectrums are measured and analyzed in the two cases: with the proposed method and without the proposed method. Figure 7 shows the vibration acceleration signal spectrums of the motor housing without any vibration suppression measures. We can find that the synchronous component of the vibration acceleration is 0.0560 *g* (*g* is the acceleration of gravity). Figure 8 shows the vibration acceleration signal spectrums of the motor housing which is removing synchronous current by novel notch filter based on coordinate transformation. The synchronous component of the vibration acceleration is 0.0262 *g*. We see from these results that there is greater than 50% reduction in synchronous vibration. Therefore, experimental results clearly show that the proposed method significantly reduces the unbalance vibration of the AMB test rig.

IV. CONCLUSION

This paper presents a notch filter for the autocentering of the magnetically suspended rotors based on rotating coordinate transformation. Simulation and experimental results show that the synchronous vibration force is significantly reduced. However, we can find there is low-frequency vibration on the motor housing which is caused by the air flow when turbine blades is rotating, but we haven't found a suitable way to accurately analyze its mechanics. It still needs further research in the future.

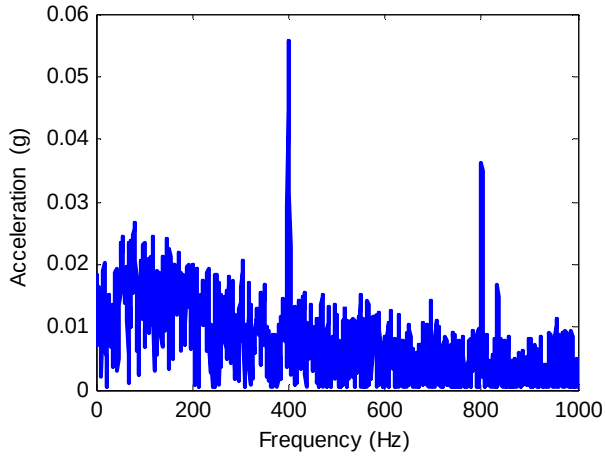

Figure 7. Vibration signal spectrum of the motor base without the proposed method

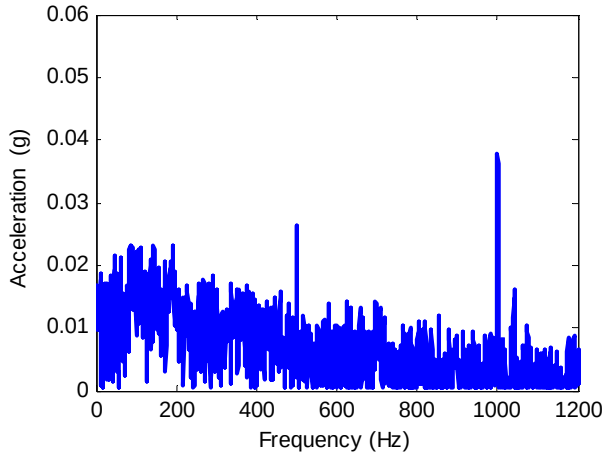

Figure 8. Vibration signal spectrum of the motor base with the proposed method

REFERENCES

[1] C. Zhu, D.A. Robb, D.J. Ewins, The dynamics of a cracked rotor with an active magnetic bearing, Journal of Sound and Vibration 265 (2003) 469–487.

[2] G. Mania, D. D. Quinna, M. Kasardab, Active health monitoring in a rotating cracked shaft using active magnetic bearings as force actuators, Journal of sound and vibration 294 (2006) 454–465.

[3] R. Herzog, P. Buhler, C. Gahler, R. Larsonneur, Unbalance compensation using generalized notch filters in the multivariable feedback of magnetic bearings, IEEE Transactions on Control System Technology 4(5) (1996) 580–586.

[4] C. Bi, D. Wu, Q. Jiang and Z. Liu, Automatic learning control for unbalance compensation in active magnetic bearings, IEEE Transactions on Magnetics 41(7) (2005) 2270–2280.

[5] Y. Maruyama, T. Mizuno, M. Takasaki, Y. Ishino, H. Kameno, and A. Kubo, Application of rotor unbalance compensation to AMB-based gyroscopic sensor, Proceedings of the 11th International Symposium on Magnetic Bearings, Nara, Japan, August 2008, pp. 206-211.

[6] K. Jiang, C. Zhu, M. Tang, A uniform control method for imbalance compensation and automation balancing in active magnetic bearing-rotor systems, ASME Journal of Dynamic Systems, Measurement, and Control 134(2) (2012) DOI: 10.1115/1.4005279, in press.

[7] L. Li, T. Shinshi, C. Iijima, X. Zhang, A. Shimokohbe, Compensation of rotor imbalance for precision rotation of a planar magnetic bearing rotor, Precision Engineering 27(2) (2003) 140–150.